TIME DEPENDENT UPWELLING IN NON-HYDROSTATIC STRATIFIED WATERS ALONG A COASTLINE

Carlos A. A. Carbonel H.
CIMATEC/SENAI, Orlando Gomes 1845, Piatã, Salvador, Bahia, Brazil

Abstract. *The hydrodynamic of stratified non hydrostatic waters is studied numerically using a stabilized finite element model. In environmental hydrodynamic, the density stratification is mainly function of the temperature and salinity structure and the internal waves are of importance for the circulation associated to low frequency fluid motions. In the present paper a particular emphasis is focused on the cross-sectional dynamics of the coastal ocean forced by a limited shear stress wind acting at the surface. The resulting motions due the steepness of the waves at the interfaces of the water layers are non-linear and non-hydrostatic phenomena. The dynamics of water flow on a continental shelf cross section will be described by a set of nonlinear dispersive equations for a layer system, also called Boussinesq type equations. To solve the model equations a finite element variational formulation is proposed. The accuracy and stability of the formulation is showed in different numerical experiments.*

Keywords: *Numerical Models; Non-Hydrostatic Waters, Upwelling, Finite Element.*

1. INTRODUCTION

The coastal upwelling is due to a wind-induced hydrodynamic divergence. The Ekman transport of the surface water away from the coast then results in a vertical motion bringing deep water to the surface. During upwelling, the internal density interface (pycnocline) has large amplitude changes in space and time with important nonlinear effects and signals of non-hydrostatic behavior. The several upwelling contributions reported in the literature have used the shallow water theory to describe upwelling phenomena. But, when the vertical acceleration is non-negligible, due path curvatures of the water particles, the pressure distribution is no longer hydrostatic and the shallow water theory is not valid. The use of Boussinesq type equations is a way to describe non-hydrostatic motions (Boussinesq, 1872). These equations are shallow water wave equations with additional third order terms.

The phenomenon of coastal upwelling of cold water in a coastal strip contributes to increase the productivity of the sea as well as to climate modifications of the adjacent land. In coastal upwelling regions, the circulation is commonly characterized by the typical formation of plumes of cold surface temperatures. The physical process of upwelling has been reviewed by Smith(1968). The upwelling is a transient phenomena and the generation and wave interaction are typical features of the phenomenon. The waves in stratified fluids play a significant role in geophysical fluid dynamics, particularly in limnology, oceanography and meteorology. Internal waves due to density variations (Gill, 1982) are responsible for producing the lowering and erosion of thermocline. Baroclinic waves influence the transport of nutrients by large amplitude wave dynamics and associated baroclinic instabilities.

While several researchers currently use finite difference approximations to deal with non-hydrostatic problems (e.g. Peregrine, 1967; Shapper and Zielke, 1984; Diebels et al., 1994b), finite element approximations are still for the most part unexplored. Also, coastal upwelling studies have used mostly finite difference methods. The present paper is a step in the study of coastal upwelling dynamics in stratified fluids applying a stabilized finite element formulation to approach the non-hydrostatic upwelling equations numerically. The method is attractive due its properties of accuracy as the selective dissipation at high spatial frequencies, controlling the spurious oscillation (Carbonel, Galeão and Loula, 2000, Carbonel and Galeão, 2004 and 2008).

A layer model is developed to describe the upwelling governed by non-hydrostatic equations in a two-layer coastal ocean using a proposed finite element model. The coastal ocean is flowing on a continental shelf cross section near a coastline in the southern hemisphere. The coastal flow is on an f plane and longshore variations are neglected. The near-shore circulation is induced into the stratified ocean by surface winds. The variables in the numerical model are described by linear polynomial. The numerical experiments are oriented to the simulation of time dependent near-shore circulation for two different bottom topographies.

2. THE UPWELLING GOVERNING EQUATIONS

It is considered a stably stratified, rotating and incompressible fluid on a continental shelf cross section along a coastline in the southern hemisphere. It is supposed that the fluid consists of two layers. In the model it is assumed that longshore variation are neglected $(\partial/\partial y)$ and the influence of the Coriolis and eddy stresses are important in the resulting dynamics. The coastal dynamics is forced by the wind acting longshore on the surface where the atmospheric pressure is uniform. In the present approach the thermodynamic effects are excluded.

For two layers of fluids the dimensional non-hydrostatic equations of continuity and motion could be written in function of the mean velocities in the upper and lower layers layers $\bar{u}_1$, $\bar{v}_1$, $\bar{u}_2$, $\bar{v}_2$ and the surface and interface levels η_0, η_1,

$$\frac{\partial \eta_0}{\partial t} - \frac{\partial \eta_1}{\partial t} + (\eta_0 + h_1 - \eta_1)\frac{\partial \bar{u}_1}{\partial x} + \bar{u}_1 \frac{\partial \eta_0}{\partial x} - \bar{u}_1 \frac{\partial \eta_1}{\partial x} - w_e = 0 \tag{1}$$

$$\frac{\partial \eta_1}{\partial t} + (\eta_1 + h_2)\frac{\partial \bar{u}_2}{\partial x} + \bar{u}_2 \frac{\partial \eta_1}{\partial x} + \bar{u}_2 \frac{\partial h_2}{\partial x} + w_e = 0 \tag{2}$$

$$\frac{\partial \bar{u}_1}{\partial t} + \bar{u}_1 \frac{\partial \bar{u}_1}{\partial x} + g\frac{\partial \eta_0}{\partial x} - \frac{h_1^2}{3}\frac{\partial^3 \bar{u}_1}{\partial x^2 \partial t} - \frac{h_1 h_2}{2}\frac{\partial^3 \bar{u}_2}{\partial x^2 \partial t} - h_1 \frac{\partial h_2}{\partial x}\frac{\partial \bar{u}_2}{\partial x \partial t} - f\bar{v}_1 - A_H \frac{\partial^2 \bar{u}_1}{\partial x^2} = 0 \tag{3}$$

$$\frac{\partial \bar{v}_1}{\partial t} + \bar{u}_1 \frac{\partial \bar{v}_1}{\partial x} + f\bar{u}_1 - A_H \frac{\partial^2 \bar{v}_1}{\partial x^2} + \frac{(\tau_y^I - \tau_y^S)}{\rho_1 h_1^*} = 0 \tag{4}$$

$$\frac{\partial \bar{u}_2}{\partial t} + \bar{u}_2 \frac{\partial \bar{u}_2}{\partial x} + g\delta\frac{\partial \eta_0}{\partial x} + g(1-\delta)\frac{\partial \eta_1}{\partial x} - \delta\frac{h_1^2}{2}\frac{\partial^3 \bar{u}_1}{\partial x^2 \partial t} - (\delta h_1 h_2 + \frac{h_2^2}{3})\frac{\partial^3 \bar{u}_2}{\partial x^2 \partial t}$$
$$- (\delta h_1 + \frac{h_2}{2})\frac{\partial h_2}{\partial x}\frac{\partial \bar{u}_2}{\partial x \partial t} - f\bar{v}_2 - A_H \frac{\partial^2 \bar{u}_2}{\partial x^2} = 0 \tag{5}$$

$$\frac{\partial \bar{v}_2}{\partial t} + \bar{u}_2 \frac{\partial \bar{v}_2}{\partial x} + f\bar{u}_2 - A_H \frac{\partial^2 \bar{v}_2}{\partial x^2} + \frac{(\tau_y^B - \tau_y^I)}{\rho_2 h_2^*} = 0 \tag{6}$$

where, the spatial and temporal coordinates are denoted by x and t respectively. The vertical structure of the coastal ocean is presented in Figure 1. The total depth is denoted by $H = h_1 + h_2(x)$, $\eta_0(x,t)$ is the water surface level and $\eta_1(x,t)$ is the interface level. The free surface is $z = \eta_0$, the interface is at $z = -h_1 + \eta_1$ and the bottom is $z = -h_1 - h_2(x)$. The instant thickness of the layers are $h_1^* = (\eta_0 + h_1 - \eta_1)$ and $h_2^* = (h_2 + \eta_1)$. The upper layer velocity components are $\bar{u}_1$, $\bar{v}_1$, and $\bar{u}_2$, $\bar{v}_2$ are the lower layer velocity components. The parameter A_H is the horizontal eddy viscosity, f is the Coriolis parameter and g is the acceleration of the gravity. The ratio between the densities is represented by $\delta = \rho_1/\rho_2$.

The hydrodynamic layer models have time integration restrictions when the internal interface reaches the surface and are not adequate to study the evolution of a surface front. A way to overcome the problem of the internal interface reaching the surface is to include the entrainment, a physical-based vertical turbulent mass transfer. Entrainment is the mass transfer from a non turbulent layer (or less turbulent) into a turbulent upper layer by surface action of the wind. A consequence is the deepening of the upper layer. The entrainment velocity w_e is represented by a convenient relation $w_e = (H_{eq} - h_1^*)^2/t_e.H_{eq}$ (Mc Creary and Kundu, 1988), t_e and H_e are the time scale and thickness of effective entrainment.

The hydrodynamic layers are coupled through the pressure gradient forces and the shear stresses, namely wind shear stress at the surface $\tau_S = \rho_{air} C_S W|W|$, the interface shear stress $\tau_I = \rho_{12} C_I(\bar{v}_1 - \bar{v}_2)|V_1 - V_2|$ and the bottom stress $\tau_B = \rho_2 C_B \bar{v}_2|V_2|$, where $V_1 = (\bar{u}_1, \bar{v}_1)$, $V_2 = (\bar{u}_2, \bar{v}_2)$ are vector velocities at the upper and lower layer respectively.

In the equations (3) and (5) the third order terms describe the dispersive features of the dynamics. In the case of Boussinesq type equations, the non linear and dispersive terms are of the same order of importance and play an important role in the solutions. The equations (1) to (6) are based on the derived equations of Diebels (1991) considering additionally the effects of entrainment, eddy viscosity and shear stresses at the surface and interface.
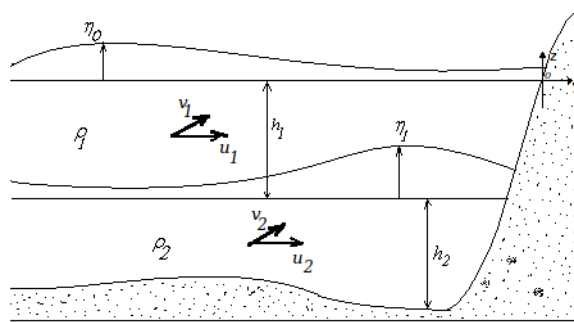

Figure 1. Vertical structure of the two-layer model with free surface, one interface and botom topography.

3. THE FINITE ELEMENT MODEL

The one dimensional spacial domain Ω is partitioned in N subdomains $\Omega_e = [x_i, x_{i+1}]$, where x_i, x_{i+1} belong to an ordered partition of space level

$$0 = x_1 < x_2 < x_3 .... < x_N = L \tag{7}$$

and the time domain is also partinionated into subintervals $[t^n, t^{n+1}]$ of lenght Δt, where the time levels belong to an ordered partition of time levels

$$0 = t^0 < t^1 < t^2 < .... < t^M = T \tag{8}$$

The governing equations presented in (1) to (6) could be written for convenience as a equation system in matrix form resulting

$$F\frac{\partial U}{\partial t} + A\frac{\partial U}{\partial x} + B\frac{\partial^3 U}{\partial x^2 \partial t} + C\frac{\partial^2 U}{\partial x \partial t} + DU + E\frac{\partial^2 U}{\partial x^2} + R = 0 \tag{9}$$

where the matrix A, B, C, D, E, F are coefficient matrix , U is the unknown vector and R is the last vector according to the following definition:

$$F = \begin{pmatrix} 1 & 0 & 0 & 0 & 0 & 0 \\ 0 & 1 & 0 & 0 & 0 & 0 \\ 0 & 0 & 1 & 0 & 0 & -1 \\ 0 & 0 & 0 & 1 & 0 & 0 \\ 0 & 0 & 0 & 0 & 1 & 0 \\ 0 & 0 & 0 & 0 & 0 & 1 \end{pmatrix}, \quad U = \begin{pmatrix} u_1 \\ v_1 \\ \eta_0 \\ u_2 \\ v_2 \\ \eta_1 \end{pmatrix}, \quad \mathcal{R} = \begin{pmatrix} 0 \\ (\tau_y^I - \tau_y^S)/\rho_1 h_1^* \\ -w_e \\ 0 \\ (\tau_y^B - \tau_y^I)/\rho_2 h_2^* \\ \bar{u}_2 \frac{\partial h_2}{\partial x} + w_e \end{pmatrix}$$

$$A = \begin{pmatrix} \bar{u}_1 & 0 & g & 0 & 0 & 0 \\ 0 & \bar{u}_1 & 0 & 0 & 0 & 0 \\ (\eta_0 + h_1 - \eta_1) & 0 & \bar{u}_1 & 0 & 0 & -\bar{u}_1 \\ 0 & 0 & g\delta & \bar{u}_2 & 0 & g(1-\delta) \\ 0 & 0 & 0 & 0 & \bar{u}_2 & 0 \\ 0 & 0 & 0 & (h_2 + \eta_1) & 0 & \bar{u}_2 \end{pmatrix}, \quad B = \begin{pmatrix} -\frac{h_1^2}{3} & 0 & 0 & -\frac{h_1 h_2}{2} & 0 & 0 \\ 0 & 0 & 0 & 0 & 0 & 0 \\ 0 & 0 & 0 & 0 & 0 & 0 \\ -\delta\frac{h_1^2}{2} & 0 & 0 & -(\delta h_1 h_2 + \frac{h_2^2}{3}) & 0 & 0 \\ 0 & 0 & 0 & 0 & 0 & 0 \\ 0 & 0 & 0 & 0 & 0 & 0 \end{pmatrix}$$

$$C = \begin{pmatrix} 0 & 0 & 0 & -h_1\frac{\partial h_2}{\partial x} & 0 & 0 \\ 0 & 0 & 0 & 0 & 0 & 0 \\ 0 & 0 & 0 & 0 & 0 & 0 \\ 0 & 0 & 0 & -(\delta h_1 + \frac{h_2}{2})\frac{\partial h_2}{\partial x} & 0 & 0 \\ 0 & 0 & 0 & 0 & 0 & 0 \\ 0 & 0 & 0 & 0 & 0 & 0 \end{pmatrix}, D = \begin{pmatrix} 0 & -f & 0 & 0 & 0 & 0 \\ f & 0 & 0 & 0 & 0 & 0 \\ 0 & 0 & 0 & 0 & 0 & 0 \\ 0 & 0 & 0 & 0 & -f & 0 \\ 0 & 0 & 0 & f & 0 & 0 \\ 0 & 0 & 0 & 0 & 0 & 0 \end{pmatrix}, E = \begin{pmatrix} -A_H & 0 & 0 & 0 & 0 & 0 \\ 0 & -A_H & 0 & 0 & 0 & 0 \\ 0 & 0 & 0 & 0 & 0 & 0 \\ 0 & 0 & 0 & -A_H & 0 & 0 \\ 0 & 0 & 0 & 0 & -A_H & 0 \\ 0 & 0 & 0 & 0 & 0 & 0 \end{pmatrix}$$

We define a finite-dimensional trial solution space $\mathcal{S}^h$ and a test function space $\mathcal{V}^h$ and we will say that the discrete Petrov-Galerkin approximate solution for the non-hydrostatic system problem (9) is the vector $\mathcal{U} \in \mathcal{S}^h$ (of piecewise polynomials), such that $p \in \mathcal{V}^h$, which satisfies the following variational formulation

$$\int_\Omega p_j \cdot (F\frac{\partial \mathcal{U}}{\partial t} + A\frac{\partial \mathcal{U}}{\partial x} + B\frac{\partial^3 \mathcal{U}}{\partial x^2 \partial t} + C\frac{\partial^2 \mathcal{U}}{\partial x \partial t} + DU + E\frac{\partial^2 U}{\partial x^2} + \mathcal{R})d\Omega = 0 \qquad (10)$$

where the weighting function p_j is defines

$$p_j = \Phi_j + \Psi A\frac{\partial \Phi_j}{\partial x} \qquad (11)$$

The matrix Ψ contains the free parameters (knows as upwind functions according to Hughes and Mallet, 1986). Here, the stabilizing matrix will be approximated by the matrix $\Psi = \tau I$, where τ is the intrinsic time scale free parameter and I is unit matrix.

The variational formulation reads

$$\int_\Omega (\Phi_j + \Psi A\frac{\partial \Phi_j}{\partial x})^T \cdot [(F\Phi_i + B\frac{\partial^2 \Phi_i}{\partial x^2} + C\frac{\partial \Phi_i}{\partial x})\frac{\partial \mathcal{U}_i}{\partial t} + (A\frac{\partial \Phi_i}{\partial x} + D + E\frac{\partial^2 \Phi_i}{\partial x^2})\mathcal{U}_i + \mathcal{R}]d\Omega = 0 \qquad (12)$$

integrating by parts results

$$\int_\Omega (\Phi_j + \Psi A\frac{\partial \Phi_j}{\partial x})^T \cdot [(F\Phi_i + C\frac{\partial \Phi_i}{\partial x})\frac{\partial \mathcal{U}_i}{\partial t} + (A\frac{\partial \Phi_i}{\partial x} + D)\mathcal{U}_i + \mathcal{R}]d\Omega$$
$$- \int_\Omega (\frac{\partial \Phi_j}{\partial x}B\frac{\partial \Phi_i}{\partial x})\frac{\partial \mathcal{U}_i}{\partial t}d\Omega + (\Phi_j B\frac{\partial \Phi_i}{\partial x}\Big|_{x=\Gamma})\frac{\partial \mathcal{U}_i}{\partial t}$$
$$- \int_\Omega (\frac{\partial \Phi_j}{\partial x}E\frac{\partial \Phi_i}{\partial x})\mathcal{U}_i \, d\Omega + (\Phi_j E\frac{\partial \Phi_i}{\partial x}\Big|_{x=\Gamma})\mathcal{U}_i = 0 \qquad (13)$$

which could be written in matrix form

$$\mathbb{M}\frac{\partial \mathcal{U}_i}{\partial t} + \mathbb{N}\mathcal{U}_i + \mathbb{R} = 0 \qquad (14)$$

where the matrices $\mathbf{M, N}$ and the vector $\mathbf{R}$ are

$$\mathbb{M} = \int_\Omega (\Phi_j + \Psi A\frac{\partial \Phi_j}{\partial x})^T \cdot (F\Phi_i + C\frac{\partial \Phi_i}{\partial x})d\Omega - \int_\Omega (\frac{\partial \Phi_j}{\partial x}B\frac{\partial \Phi_i}{\partial x})d\Omega + (\Phi_j B\frac{\partial \Phi_i}{\partial x}\Big|_{x=\Gamma}) \qquad (15)$$

$$\mathbb{N} = \int_{\Omega} (\Phi_j + \Psi A \frac{\partial \Phi_j}{\partial x})^T \cdot (A \frac{\partial \Phi_i}{\partial x} + D\Phi_i) d\Omega - \int_{\Omega} (\frac{\partial \Phi_j}{\partial x} E \frac{\partial \Phi_i}{\partial x}) d\Omega + (\Phi_j E \frac{\partial \Phi_i}{\partial x}\bigg|_{x=\Gamma}) \tag{16}$$

$$\mathbb{R} = \int_{\Omega} [\Phi_j + \Psi A \frac{\partial \Phi_j}{\partial x}]^T \cdot \mathcal{R} \, d\Omega \tag{17}$$

The time approximation of equation (14) is obtained for $\mathcal{U}(t)$ defining a linear approach between two time levels

$$\mathcal{U}(t) = \theta \mathcal{U}^{n+1} + (1-\theta)\mathcal{U}^n \tag{18}$$

where

$$\theta = \frac{t - t^n}{t^{n+1} - t^n} \tag{19}$$

Defining

$$\frac{d}{dt}\mathcal{U}(t) = \frac{1}{\Delta t}(\mathcal{U}^{n+1} - \mathcal{U}^n) \tag{20}$$

then, the final system equation reads

$$\mathbb{M} \frac{1}{\Delta t}(\mathcal{U}^{n+1} - \mathcal{U}^n) + \mathbb{N}(\theta \mathcal{U}^{n+1} + (1-\theta)\mathcal{U}^n) + \mathbb{R} = 0 \tag{21}$$

or also

$$\mathcal{M}\mathcal{U}^{n+1} + \mathcal{N}\mathcal{U}^n + \mathbb{R} = 0 \tag{22}$$

where

$$\mathcal{M} = \mathbb{M} \frac{1}{\Delta t} + \mathbb{N}\theta \quad , \quad \mathcal{N} = -\mathbb{M} \frac{1}{\Delta t} + \mathbb{N}(1-\theta) \tag{23}$$

4. NUMERICAL EXPERIMENTS

In the present section, numerical experiments are concerned with the onset of upwelling and the time dependent response of the stratified water forced by winds. The response of coastal dynamics is explored using two different shelf case configurations.

4.1 Flat-Shelf case experiment

In the present case, a steady alongshore wind (W_y=10ms^{-1}) blows in a coastal band of 200km ($x \in [0, -200\text{km}]$) and drops rapidly in magnitude 200km off the coast (Figure 2). The continental shelf of constant depth 200m with $h_1 = 50m$ and $h_2 = 150m$. The value of the Coriolis parameter is $f = -10^{-4}\text{sec}^{-1}$, the gravity aceleration is $g = 10\text{ms}^{-2}$, the eddy viscosity is $A = 100m^2 s^{-1}$. The fluid densities are defined as $\rho_1 = 1022\text{kgm}^{-3}$, $\rho_2 = 1024\text{kgm}^{-3}$. The friction parameters are $C_S = 0.001$, $C_I = 0.0003$, and $C_B = 0.0003$. The numerical coeeficient is $\theta = 2/3$ and the intrinsic time scale is $\tau = 1s$. The entrainment is not considered in this experiment.
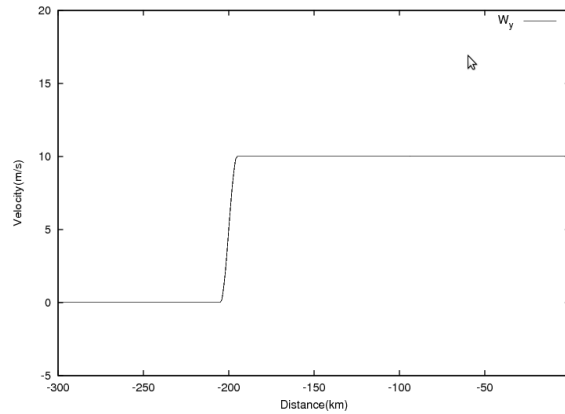
Figure 2. Longshore wind component variation in function of the distance from the shore.

The model is initially at rest with $h_1 = 50m$ and $h_2 = 150m$ for all x. At time $t=0$ a longshore wind is impulsively applied. The model is integrated in time during 8 days. The velocities and interface levels changes will be evaluated using the non-hydrostatic model presented in section 3.

When the model is forced by the steady alongshore wind (W_y) presented in Figure 2, an upwelling coastal band is generated near the coastline by a one-sided divergence of waters in the upper layer (due the Coriolis force an Ekman flow occurs in direction -x), resulting the shoaling of the upper layer thickness near the shore. The conservation of mass in the vertical structure requires a compensating flow from the lower layer; thus the thickness of the lower layer increases and a convergence motion occurs with a mass flow directed to the shore. Additionally a downwelling sector is generated in the offshore side compensating the mass conservation in the coastal section.

The Figure 3 illustrates the response of the model to the wind forcing, showing the velocity components and the surface and interface levels after 4 day as a function of x.

The velocity profiles as function of x are showed in Figure 3(Left). The upper layer velocity u_1 is oriented offshore (one-sided divergence motion) whereas the lower layer u_2 is onshore oriented (convergence motion). The longshore velocities (v_1 and v_2) are oriented in the positive direction of y. It could be observed that in the band between the 50 to 150km from the coast, the longhore velocities are practically identical indicating a barotropic structure. In the band from 0 to 50km and 150km to 250km from the coast, the longshore velocity profiles indicate a baroclinic structure(larger magnitude in the upper layer than in the lower layer).

The anomalies of the surface and interface level at day 4 are showed in Figure 3 (Right). The interface has surfaced in a band near the shore (0 to 30km from the coast) due divergence of surface water in the upper layer and convergence motion in the lower layer. Near the 200km from the coast a downwelling sector is observed due the convergence flow in the upper layer and divergence flow in the lower layer.
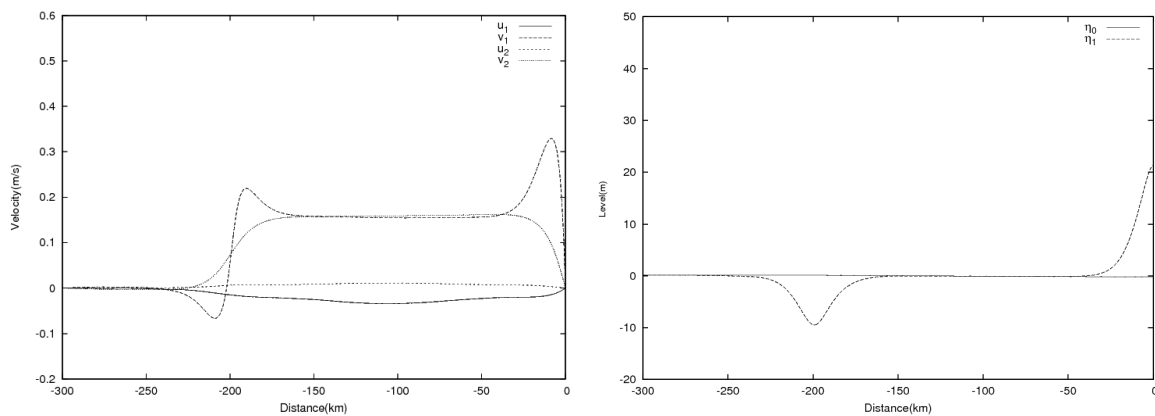

Figure 3. Flat-Shelf Case. Variable profiles after 4 days as a function of x. Velocity profiles (Left). Interface level and surface level anomaly (Right). The surface jet occurs near $x=0$ and positive interface anomaly indicates upwelling.

In the Figure 4 (Left) the evolution of the velocity profiles during 8 days is presented. The velocity profiles have a similar format but increasing the magnitude with the time. The inertial oscillations are a feature of unsteady circulation and the uneven spacing of the lines indicates the presence of these waves. Near the coastline the coastal Jet is well developed. A weak counter-current is observed from the 200km to 250km from the coast. The evolution of the interface level is presented in Figure 4 (Right) reaching an anomaly of 38m near the shore at day 8. The interface level in the downwelling zone reaches an anomaly of 17m negative.
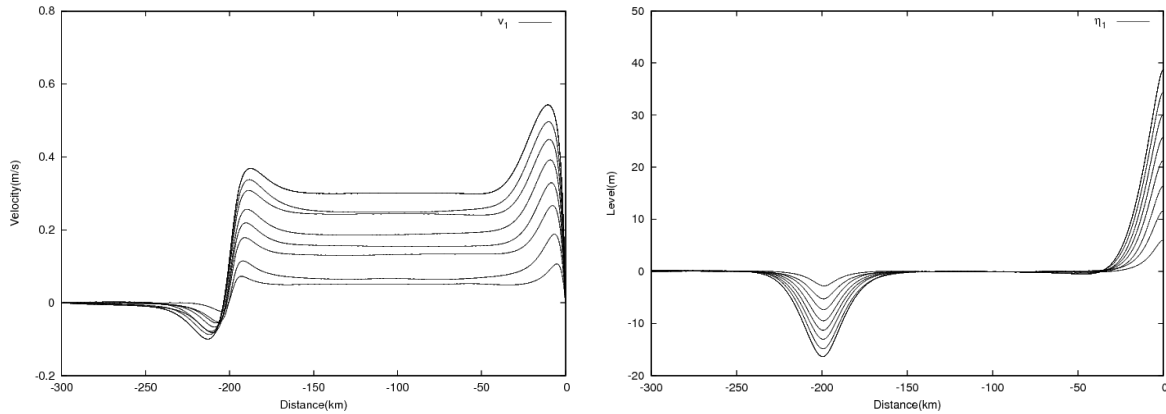

Figure 4. Flat-Shelf Case. Distribution of variables as a function of x for 8 days. Upper layer velocity v_1 for each day(Left). Interface high anomaly for each day(Right).

In the presented numerical results, the baroclinic coastal jet observed in the band of 0 to 50km from the coast is the most interesting phenomena. The coastal Jet is a feature reported in the literature by time dependent studies (e.g. O'Brien and Hulburt, 1972; Csanady 1968). The Jet appears during the initial stages of the hydrodynamic response of the coastal waters to an impulsively applied alongshore wind stress and is associated to the Rossby radius of deformation of around 20km (Allen, 1973) in the present case.

The presence of a weak counter-current from -250km to -200km could be explained observing the motion equation (4) where the $\frac{\partial v_1}{\partial t}$ is negative during the simulation in this sector. The wind forcing is zero in the indicated sector and since the initial stages, the term $f u_1$ (positive) is more important in the momentum transfer equation inducing negative values of v_1. Later $u_1 \frac{\partial v_1}{\partial x}$ (will be positive) contributes to increase the magnitude of the weak counter-current.

4.2 Sharp-Shelf case experiment

This numerical experiment deals with a sharp-shelf configuration. In the present case the continental shelf is 200m depth but shoreward of 100km there exists a shallow inshore shelf of 64m depth (Figure 5).
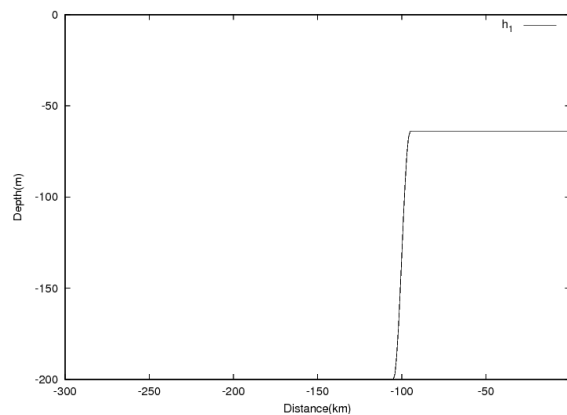

Figure 5. Bottom topography of the sharp-shelf case

The upper layer thickness is defined at 50m depth at $t = 0$. The wind forcing structure is identical to the previous case (Figure 2). The model is integrated in time during 8 days.

In Figure 6(Left), the velocity components, as a function of x, are shown after 4 days the wind is blowing. The upper layer velocity u_1 is oriented offshore whereas the lower layer u_2 is onshore oriented. The inshore velocity u_2 increases as the bottom rises near 100km from the coast. It is observed that longshore velocity components in the band between the 40 to 70km and 130 to 170km from the coast have a barotropic structure, whereas in the band form 0 to 30km, 70 to 130km and 160km to 240km the velocity structure is baroclinic. The baroclinic structure is associated to the upwelling and downwelling phenomena producing anomalies (Figure 6, Right) at the interface near the shore, at 100km from the coast (secondary upwelling) and at 200km from the coast (downwelling sector).

The Figure 7(Left) shows the velocity profiles evolution during the 8 days. Near the coast the coastal Jet is the more important feature. A weak surface counter-current is also observed from the 200-250km. The longshore velocity component has larger magnitudes from the 40km to 100km from the coast compared to the values obtained in the previous flat-shelf case.

The Figure 7(Right) shows the interface evolution during the 8 days. A weak secondary upwelling region appears at 100km from the shore, in the sector of the sharp-shelf topography change. The secondary upwelling is a dynamic feature observed in the nature and explained by the conservation of the potential vorticity, as indicated by O'Brien and Hulburt (1972). The interface level reaches an anomaly of 28m at day 8, a smaller value compared to the obtained for the flat-shelf case (38m). The main reason is the smaller inshore water flux due the smaller thickness of the lower layer in the sector from 0 to 100km from the coast.
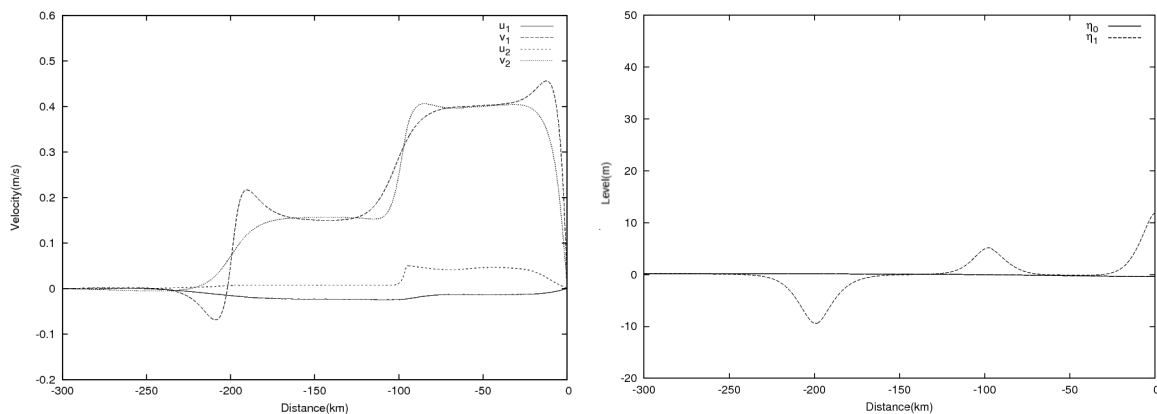

Figure 6. Sharp-Shelf Case. Velocity component profiles after 4 days as a function of x (Left). Interface level and surface level anomaly after 4 days(Right). The surface jet occurs near $x=0$ and positive interface anomaly indicates upwelling.
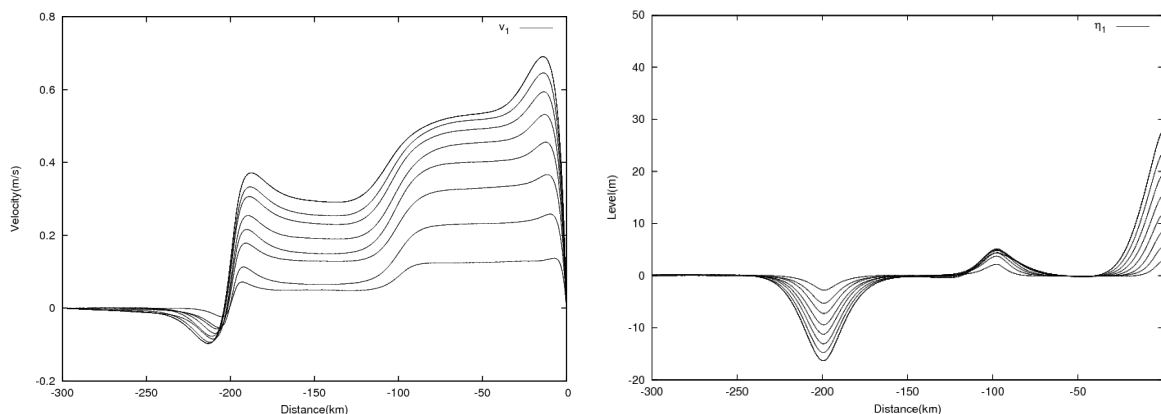

Figure 7. Sharp-Shelf Case. Distribution of variables as a function of x for 8 days. Upper layer velocity v_1 for each day (Left). Interface level anomaly for each day (Right).

4.3 Time dependent wind forcing

In this experiment, the sharp-shelf configuration is forced by a time dependent longshore wind W represented by a sinus wave

$$W = W_{\text{bas}} + W_{\text{amp}} \sin(2\pi t/T) \tag{24}$$

where t is the time; the parameter W_{bas} is the wind basic magnitude, W_{amp} is the amplitude and T is the period of wind magnitude oscillation, defined equal to 10ms^{-1}, 1ms^{-1} and 6 days respectively.

Initially the model is at rest and the wind function is applied at time $t=0$. The model is integrated in time during 20 days using the same parameters of the sharp-shelf case. The entrainment effect was included in this experiment using $H_{\text{eq}} = 30m$ and $t_e = 1/4$ day giving a physical control of the outcropping of the interface in this kind of models.

The time evolution of the upper layer thickness and velocity component are presented in Figure 8. The interface level at the shore (Figure 8, Left) shows an evolution with a clear influence of the wind oscillation. At a control point located at 10km from the shore the time history of the velocities is presented in Figure 8(Right). The longshore velocity components have maximal values around the 0.7ms^{-1} in the upper layer.
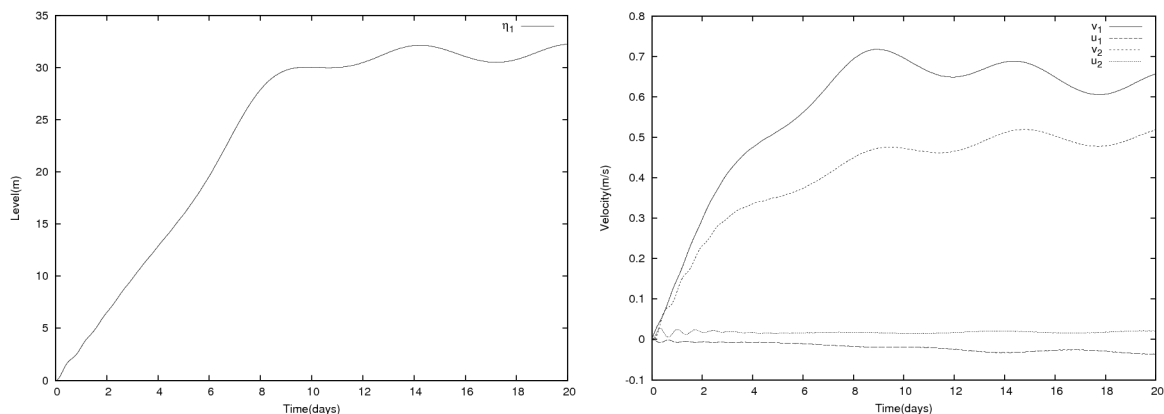

Figure 8. Time history of interface level and velocities at control points during 20 days. (Left) Interface level anomaly at the shore. (Right)Velocity components at 10km from the shore.

Two kinds of oscillations are observed in the time history of the variables near the shore (Figure 8). After 6 days the interface reaches a level of around 30m. This level is maintained due the influence of the entrainment deepening the interface and acting against vertical advection. The observed long period oscillations of around 6 days of period are associated to the wind oscillation T. The short period oscillations of around 1 day of period (more visible during the first days in the cross-shore velocity components) are associated to the inertial waves excited during the initial setup of the model. Near the coast such inertial oscillations are rapidly damped by friction and mixing processes.

5. SUMMARY AND CONCLUSIONS

A two layer finite element model of coastal upwelling taking into account the non-hydrostatic behavior of the waters has been formulated. The equation system is based on Boussinesq type equations for non linear dispersive hydrodynamic and it is assumed that longshore variation are neglected $(\partial/\partial y=0)$. The model includes the influence of the topography changes, Coriolis effect, eddy stresses due turbulence and entrainment between the layers. To solve the non hydrostatic governing equations of the two-layer model, a stabilized finite element variational formulation is presented.

The experiments are focused on the cross-sectional dynamics of the coastal ocean forced by a limited shear stress wind acting at the surface. It is studied the non-steady response of the waters for continental shelf cross sections, a flat shelf case and a sharp-shelf case. The results shown some typical features of upwelling coastal configurations. A coastal jet is generated and confined to a band near the shore. The presence of downwelling is obtained in each case. The changes of the continental shelf (Sharp-Shelf case) influences the resulting dynamics generating a secondary upwelling.

REFERENCES

Allen J. S. 1973. "Upwelling and costal jets in a continuously stratified ocean" . Journal of Physical Oceanography, vol. 3, NO 3, 245-257.

Abbot M.B.,Peterson H.M., Skoovgaard, 1978. "On the Numerical Modelling of Short Waves in Shallow Water". Journal of Hydraulic Research, 16, 173-203.

Brooks A.N., Hughes T., 1982. "Streamline upwind Petrov-Galerkin formulations for convection-dominated flows with particular emphasis on the incompressible Navier-Stokes equations". Comput. Meths. Appl. Mech. Engrg. 32, pp. 199-259.

Carbonel C., Galeão A.C., Loula A., 2000. "Numerical Study of Petrov-Galerkin Formulations for the Shallow Water Wave Equations". Journal of the Brazilian Society of Mechanical Sciences, Vol. XXII, No 2,   pp 231-247.

Carbonel C.. e A. C. N. Galeão, 2004. "A One-Dimensional Finite Element Model for Non-Hydrostatic Water Waves in Shallow Waters". Proceedings of the XXV Iberian Latin-American Congress on Computational Methods in Engineering. CILAMCE 2004. Recife, Brasil, Nov. 12 -14, 2004. Paper CIL08-009.

Carbonel C.. e A. C. N. Galeão, 2008. A Finite Element Model for Nonlinear Dispersive Dynamics in Stratified Waters. Proceedings of the XXIX Iberian Latin-American Congress on Computational Methods in Engineering. 2008 (Maceió, 4-7 Novembro 2008).

Csanady G.T.,1968. "Motions in a model great lake due to a suddenly imposed wind". Journal of Geophysical Research, 73, 6435-6447.

Diebels S., 1991. "Interne Wellen. Ein Modell, das Nichtlinearitaet, Dispersion, Corioliseffecte und variable Topographie beruecksichtigt". Doctoral Thesis, Technische Hochschule Darmstadt, 173pp.

Diebels S., Schuster B. and Hutter K.,1994a. "Nonlinear internal waves over variable topography". Geophys. Astrophys. Fluid Dynamics, Vol 76, pp. 165-192.

Diebels S., Schuster B. and Hutter K.,1994b. "Viscous effects in internal waves of two-layered fluids with variable depth". Eur. J. Mech., B/Fluids, 15, no 4, pp. 445-470.

Gill A., 1982. Atmosphere-Ocean Dynamics. Academic Press Inc. 688pag.

Hauguel A, 1980. "Adaptation of tidal numerical models to shallow water wave problems". Proc. 17th Coastal Engineering Conf., Sidney Australia.

Hughes T., Mallet M., 1986. "Finite Element Formulation for Computational Fluid Dynamics: III. The Generalized Streamline operator for Multidimensional Advective-Diffusive Sysems". Comput. Meths. Appl. Mech. Engrg., Vol. 58, pp. 305-328.

Liska R., B. Wendroff, 1997. "Analysis and Computation with stratified fluid models". Journal of Computational Physics, 137, 212-244.

Mc Creary J., P. Kundu, 1994. A Numerical Investigation of the Somali Current during the Southwest Monsoon. Journal of Marine research, 46, 25-58.

O' Brien J., Hurlburt H.E., 1971. "A numerical model of coastal upwelling". Journal of Physical Oceanography.Vol 2, pp14-26.

Peregrine D.H., 1967. "Long waves on a beach". Journal of Fluid Mechanics, 27, 815.

Shapper H. Zielke W., 1984. "A Numerical Solution of Boussinesq Type Wave Equations". Proc. 19th ICCE. Houston.

Smith, R.L., 1968. Upwelling. Oceanography and Marine Biology Annual Reviews 6, 11-46.